

# Computational Fluid Dynamics of Dispersed Mist Phenomenon in a Thermal Ink Jet Printer

Kazuhiro Mori

*Product Verification Center, Customer Focus & Quality Unit, Document Products & Supply Company, Fuji Xerox Co., Ltd., Ebina-shi, Kanagawa, Japan*

The dispersed mist phenomenon occurs when small ink droplets are blown up and contaminate the inside of the printer. In this paper, we numerically predict the motion of ink droplets in a confined space through Computational Fluid Dynamics to better understand this phenomenon. Our numerical calculations correlate well with our experimental results. A vortex is generated by the interaction of ink droplets and the flow field through momentum exchange. Consequently, ink droplet behavior can primarily be defined by the velocity relative to the surrounding flow field. Experiments reveal that the optical density of the dispersed mist has a minimum peak for jetting frequency. We investigate the effects of jetting frequency on misting and find that air current generated by main drops tends to transport small mist particles to the paper at higher frequencies. This explains why misting is high at low frequencies. It is shown that the nonlinear coupling between the flow field and ink droplets defines the property of the dispersed mist phenomenon in detail.

Journal of Imaging Science and Technology 47: 250–255 (2003)

## Introduction

Mist, in ink jet printing, refers to the minuscule ink droplets generated by ink ejection. Although manifestations of the dispersed mist phenomenon<sup>1</sup> have been observed in experiments, it is impossible to accurately measure the flow field in a confined space. Blumberg and Semiat<sup>2</sup> recently reported on velocity measurements of ink drops ejected from a piezoelectric DOD print head. They showed that low ejection frequency has a greater tendency to produce multiple peak distributions. Semiat<sup>3</sup> was not sure whether the low ejection frequency was responsible for increased multiple peak distributions. Physical phenomena occurring in confined spaces have generally been difficult to quantify. Therefore, we numerically predicted the motion of ink droplets in a confined space by Computational Fluid Dynamics. We used a computer program called FLUENT Ver.5.5 (Fluent Inc., Lebanon, NH, U.S.A.).

Many numerical simulations<sup>4–7</sup> have been conducted in the imaging sciences. Asai and co-workers<sup>4</sup> estimated the bubble-generation temperature and the initial bubble pressure through a one-dimensional model. Lean<sup>7</sup> reported on Acoustic Mist Imaging based on the ElectroPrint concept. However, the dispersed mist phenomenon has never been studied.

In this paper, we investigate this phenomenon by simultaneously evaluating the continuous phase flow and the discrete phase. The continuous phase flow is air and

the discrete phase is an ink droplet. The flow field in the neighborhood of the nozzles is excited by the ejection of droplets. In other words, momentum transfers from ink droplets to the flow field. We can numerically predict the steady flow field surrounding droplets through droplet diameter, velocity, the number of droplets per unit of space and the molecular viscosity of air. Satellite droplets with a finite initial velocity are ejected from nozzles. By changing the diameter of droplets, we can investigate the behavior of satellite droplets through the effects of the steady flow field.

The second section has photographs of dispersed mist and the results of our experiments. We found the vortices in the neighborhood of the nozzles. Photographs also reveal that mist circulates on the upstream side. The third section discusses the analysis model and numerical conditions. The fourth section briefly describes coupled calculations and particle trajectory calculations. We also show velocity vectors and contours of vorticity magnitude in the middle plane. Our numerical calculations correlated well with our experimental results. The fifth section has particle trajectories in a laminar flow. We found the behavior of blown up mist depended on the diameter of the satellite droplets. However, mist could not circulate on the upstream side. The numerical results revealed that droplets need upstream velocity to circulate mist on the upstream side. The sixth section discusses how we generated 200 satellite droplets and investigates the critical diameter for droplets to disperse into a mist. To conclude, we summarize the results taking into account the vortices generated by the interaction of the flow field and ink droplets.

## Photographs of Dispersed Mist and Experiments

Figures 1(a) and 1(b) are photographs of dispersed mist at a jetting frequency of 18 kHz. These photographs were taken by Dudek of the IJBU-WEST of Xerox Corporation.

Original manuscript received September 25, 2002

\*Corresponding author: Kazuhiro.Mori@fujixerox.co.jp

*Supplemental Materials—Figures 4 and 5 can be found in color on the IS&T website ([www.imaging.org](http://www.imaging.org)) for a period of no less than two years from the date of publication.*

©2003, IS&T—The Society for Imaging Science and Technology

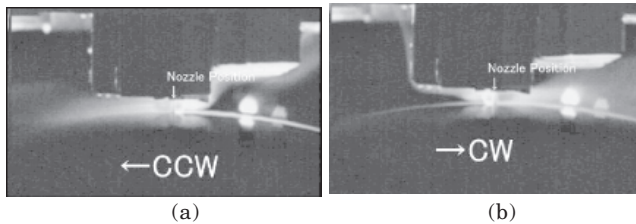


**Figure 1.** (a) Photograph of dispersed mist from nozzles. CCW means counterclockwise. (b) Photograph of dispersed mist from nozzles. CW means clockwise.

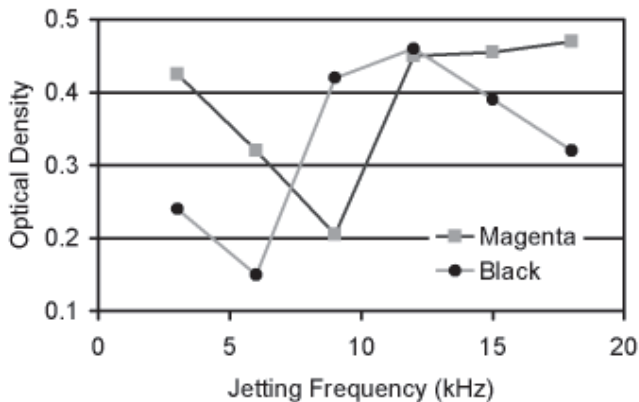


**Figure 2.** Optical density of mist patches that collected on a 5  $\mu\text{m}$  nylon filter. Ordinate axis shows optical density collected by vacuum.

We can establish the dispersed mist phenomenon through these photographs.

- The upstream vortex is small and dense.
- The downstream vortex is elongated and elliptical.
- A great deal of mist is transported downstream.

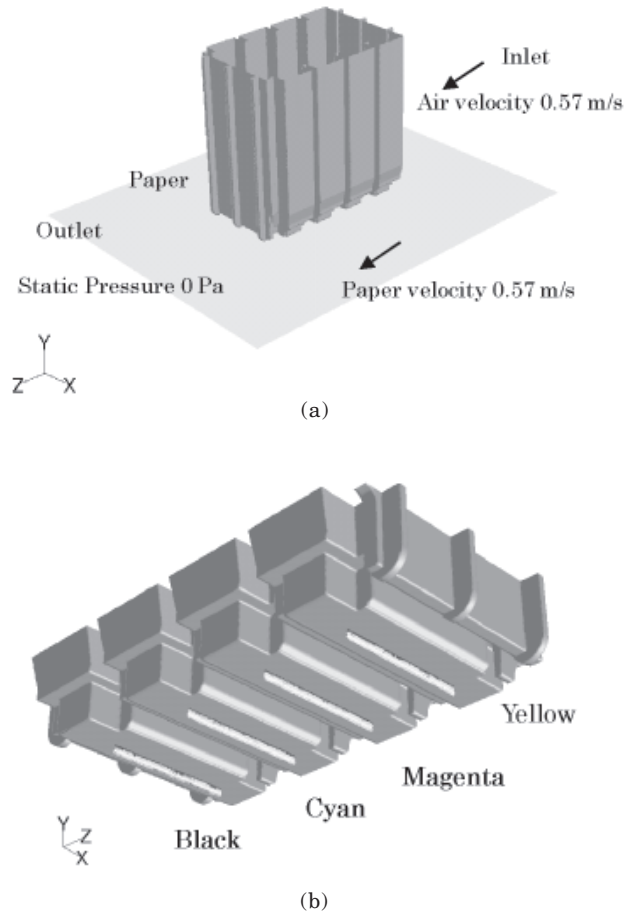
Since ink droplets are transported downstream, it is difficult to understand mist circulation on the upstream side.

Figure 2 shows the optical density of mist patches that were collected on a 5  $\mu\text{m}$  nylon filter. (Measurements were carried out by Dudek of the IJBU-WEST of Xerox Corporation.) The black ink mist reaches a minimum at a jetting frequency 6 kHz. The magenta ink mist reaches a minimum at a jetting frequency 9 kHz. Freire<sup>8</sup> assumed that the dispersed mist problem is defined by the coupling of two main physical phenomena. One is that the ink droplets appear to be unstable and a great deal of mist is generated at higher frequencies. Here, we assume that black ink nozzles exceed their manufacture specifications at jetting frequencies over 12 kHz. However, the other, the physical phenomenon at lower frequencies, is unclear. Consequently, we investigated the effects of jetting frequency on misting.

### Analysis Model and Conditions for Numerical Calculations

Figure 3(a) shows the analysis model. This model has about 2 million cells.

The analysis model consists of a rectangular prism, 191 mm long, with cross-sectional dimensions of 84 mm  $\times$  155 mm. The carriage is 85.5 mm in length, 53.5 mm in width and 82.1 mm in height. The distance between



**Figure 3.** (a). Analysis model. The carriage is static and the paper is moving for scans. (b) Carriage geometry from underneath.

the carriage and the paper is 1.9 mm. Since the carriage is static, we inversely considered the flow field and paper motion. The velocity was prescribed at the inlet boundary and the pressure was prescribed as 0 at the outlet boundary. Pressure means static gauge pressure. The paper is a no slip wall at constant velocity. The other three surfaces are free-slip walls.

We first calculated a steady flow field taking into consideration the interaction between the flow field and ink droplets. The general procedure<sup>9</sup> for solving the steady state problem is outlined below:

1. Calculate airflow.
2. Eject main and satellite droplets.
3. Calculate coupled flow.
4. Repeat until each equation converges.

Since the continuity equation does not completely satisfy the criteria, we monitored the magnitude of maximum velocity in the region of analysis and used it as the convergence criterion.

These ink droplets consist of a main droplet, a satellite droplet and an auxiliary satellite droplet. We only used black ink. The ink droplet density was 1050 kg/m<sup>3</sup>, and we ejected a total of 3000 droplets. We then investigated the behavior of small satellite droplets in the steady flow field. We assumed that the ejected droplets did not affect the steady flow field. Figure 3(b) shows

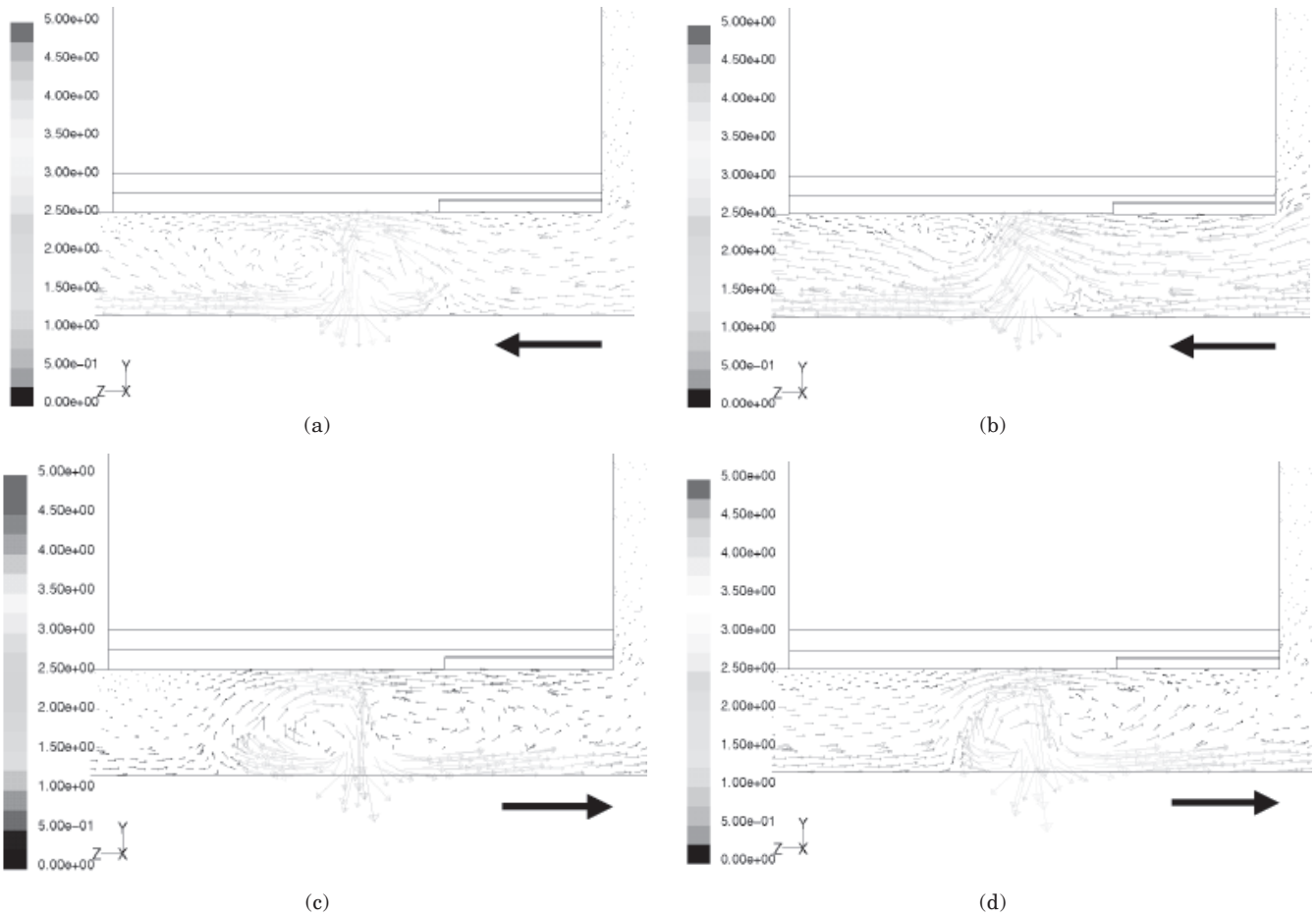


**Figure 4.** (a) Velocity vectors in middle plane for scans at 18 kHz; (b) Velocity vectors in middle plane for scans at 6 kHz; (c) Velocity vectors in middle plane for rescans at 18 kHz; (d) Velocity vectors in middle plane for rescans at 6 kHz. A full color version of this figure can be found as Supplemental Material on the IS&T website ([www.imaging.org](http://www.imaging.org)) for a period of no less than two years from the date of publication.

the carriage geometry from underneath. Our model for analysis assumes the Printhead improved by Fujii and co-workers.<sup>10</sup> Table I has the black-ink ejection conditions and Table II has the thermal ink jet operating conditions used for analysis. Ink droplets are ejected at intervals of 55  $\mu\text{s}$  at a frequency 18 kHz. The droplet flow rate is expressed in kg/s.

### Velocity Vectors and Contours of Vorticity Magnitude in Laminar Flow

In this section, we discuss velocity vectors and contours of vorticity magnitude in the middle plane without considering turbulent effects. FLUENT numerically solves Navier–Stokes equations:

$$\frac{\partial \rho}{\partial t} + \frac{\partial(\rho u_j)}{\partial x_j} = 0, \quad (1)$$

$$\frac{\partial(\rho u_i)}{\partial t} + \frac{\partial(\rho u_j u_i)}{\partial x_j} = -\frac{\partial p}{\partial x_i} + \frac{\partial}{\partial x_j} \left( \mu \frac{\partial u_i}{\partial x_j} \right) + \rho g_i, \quad (2)$$

where  $\rho$  is the fluid density,  $p$  is the static pressure, and  $x_i$  ( $i = 1, 2, 3$ ) represent the Cartesian coordinates. Here,  $u_i$  ( $i = 1, 2, 3$ ) represent the Cartesian components

of velocity  $\mathbf{u}$ ,  $g_i$  ( $i = 1, 2, 3$ ) represent the Cartesian components of gravitational acceleration  $\mathbf{g}$  and  $\mu$  is the molecular viscosity of the fluid. Here, we also adopted the Einstein convention that whenever the index appeared twice in any term, we implied summation over the range of that index. It is reasonable to assume the fluid is incompressible for this problem.

FLUENT<sup>9</sup> predicts the trajectory of a discrete phase particle by integrating the balance for the particle, which is written in a Lagrangian reference frame. This force balance equates the particle inertia with the forces acting on the particle, and can be written as

$$\frac{d\bar{u}_p}{dt} = F_D(\bar{u} - \bar{u}_p) + \frac{\rho_p - \rho}{\rho_p} \bar{g} + \bar{F}, \quad (3)$$

$$F_D = \frac{18\mu}{\rho_p D_p^2} \frac{C_D R_e}{24}. \quad (4)$$

This is where the first term to the right of Eq. (3) is drag force per unit particle, the second term is buoyancy and the third term represents additional forces. Additional forces contain the virtual mass force, or force excited due to the pressure gradient. The third term  $\mathbf{F}$

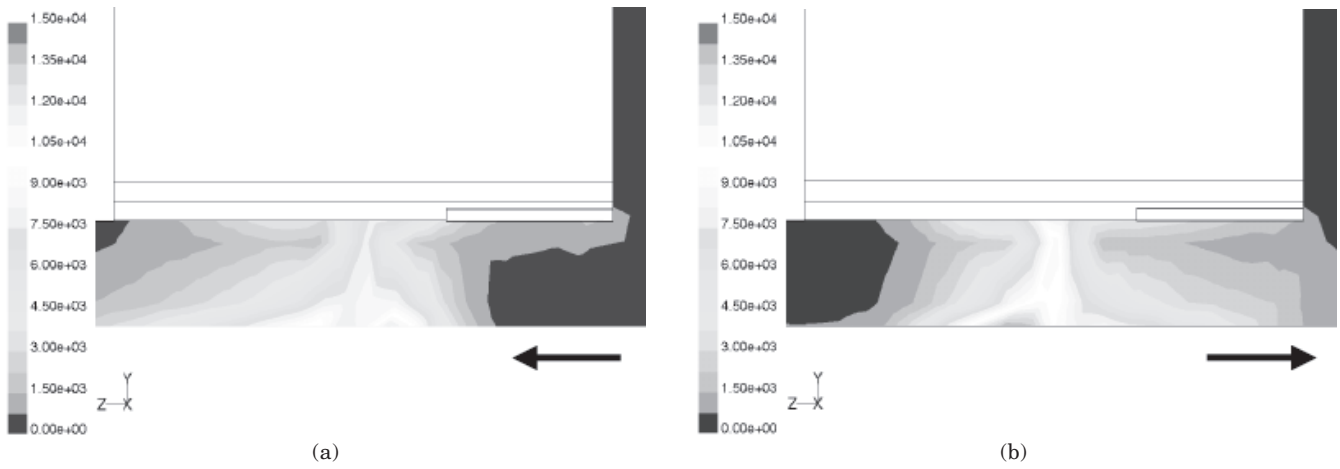


**Figure 5.** (a) Contours of vorticity magnitude in middle plane for scans at 18 kHz. (b) Contours of vorticity magnitude in middle plane for rescans at 18 kHz. A full color version of this figure can be found as Supplemental Material on the IS&T website ([www.imaging.org](http://www.imaging.org)) for a period of no less than two years from the date of publication.

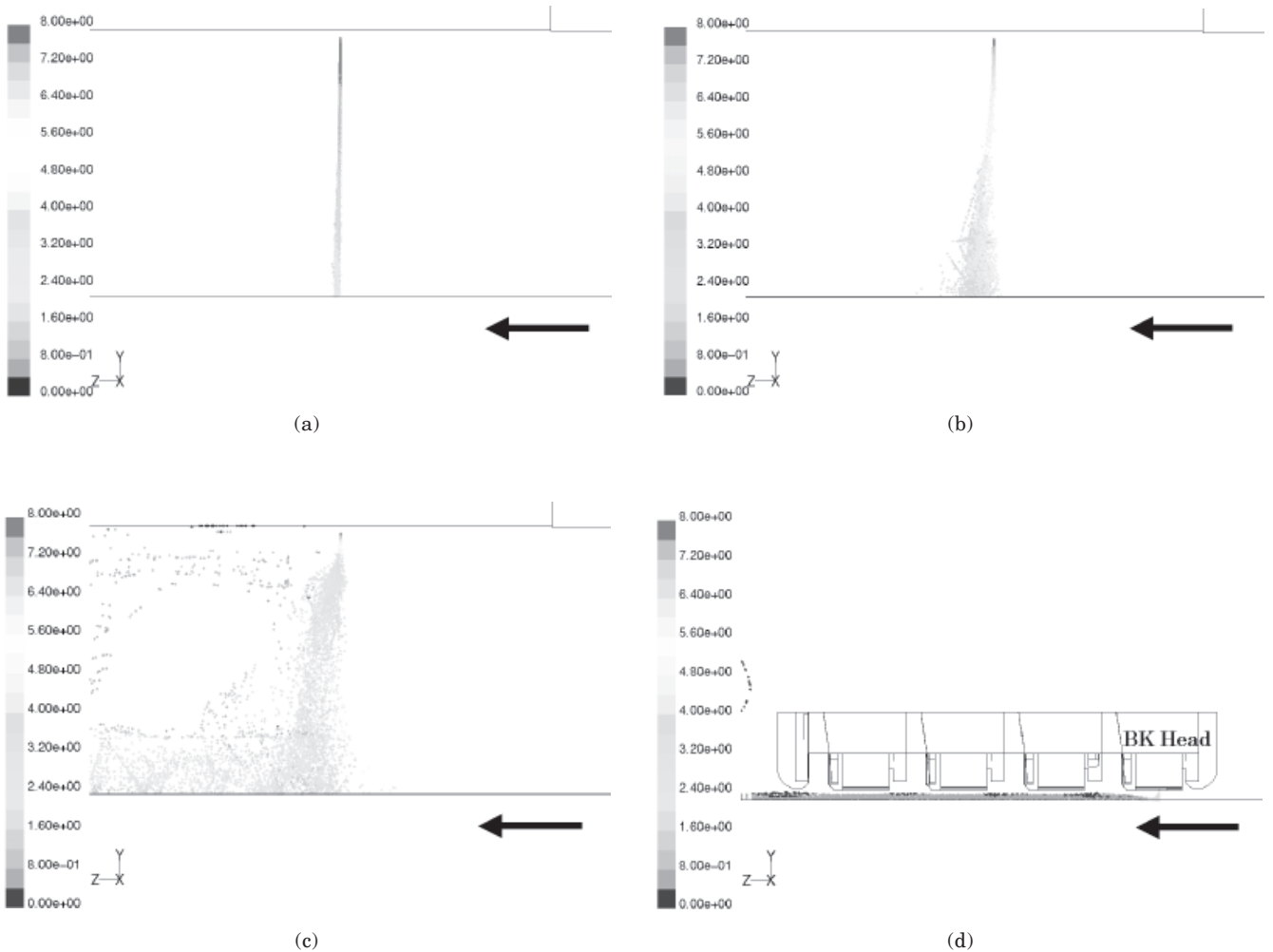


**Figure 6.** (a) Droplet trajectories for scans at 18 kHz. Droplet diameter is 18  $\mu\text{m}$  and initial velocity is  $-8$  m/s. (b) Droplet trajectories for scans at 18 kHz. Droplet diameter is 7  $\mu\text{m}$  and initial velocity is  $-8$  m/s. (c) Droplet trajectories for scans at 18 kHz. Droplet diameter is 3  $\mu\text{m}$  and initial velocity is  $-8$  m/s. (d) Droplet trajectories for scans at 18 kHz. Droplet diameter is 5  $\mu\text{m}$  and initial velocity is  $-8$  m/s.

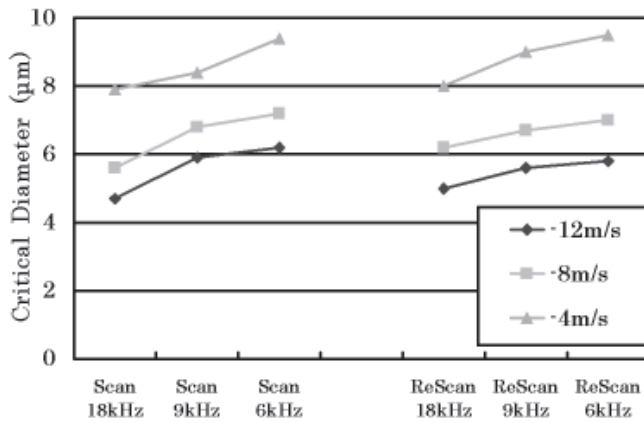


**Figure 7.** Critical diameter for initial y component velocity at  $-12$  m/s  $-8$  m/s and  $-4$  m/s.

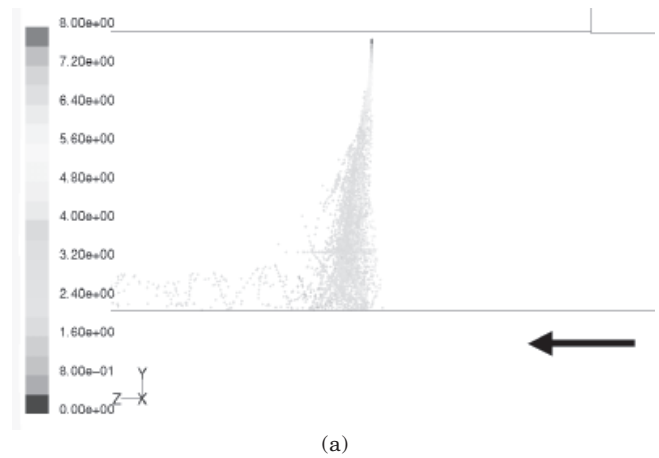
is ignored because droplet density is much greater than air density in this analysis. Here,  $\mathbf{u}_p$  is the particle velocity,  $\rho_p$  is the density of the particle, and  $D_p$  is the particle diameter.  $Re$  is the relative Reynolds number and  $C_D$  is the drag coefficient.

Table III shows the maximum values of velocity magnitude and vorticity magnitude in all cases. Both values become larger as the jetting frequency becomes larger. This means that a lot of momentum transfers from droplets to the flow at higher frequencies. We also found that both values are larger for the rescans at the same frequency. Table IV has the average velocity at four ink tank positions during scanning. This is where no main or satellite drops influence the flow. It is reasonable that the average velocity at the front is large. Black is first for the scans and fourth for the rescans. The relative velocity is probably larger for the rescans at the same frequency. Therefore, we can establish that the maximum velocity is large for the rescans at the same frequency.

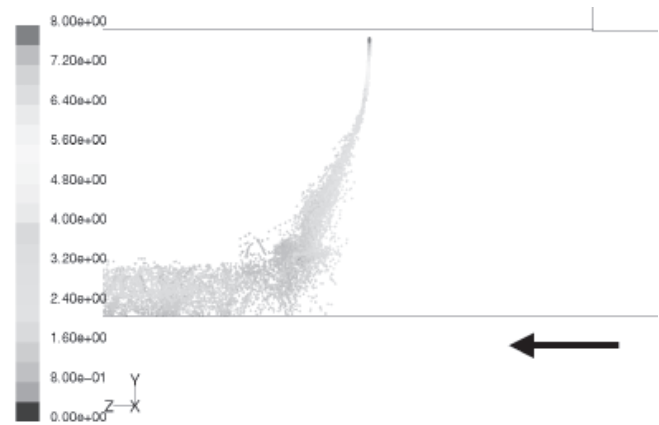
Figures 4(a) to 4(d) show velocity vectors in the neighborhood of the nozzles. In the color version of these figures, available as Supplemental Materials on the IS&T website ([www.imaging.org](http://www.imaging.org)), these vectors are colored by velocity magnitude (m/s). The symbol  $\leftarrow$  or  $\rightarrow$  in the figures shows the airflow direction. We observed vortices in the neighborhood of the nozzles. The downstream vortex is elliptical. Figures 5(a) and 5(b) show contours of vorticity magnitude. They are colored by vorticity magnitude ( $s^{-1}$ ). There is a large vorticity region on the upstream side in Figs. 5(a) and 5(b) despite the motion of the carriage.

### Particle Trajectory Calculations in a Laminar Flow

In this section, we discuss droplet trajectories in a laminar flow. We consider a case where the initial y component velocity of the satellite droplet is  $-8$  m/s for the scans at 18 kHz. Figures 6(a) to 6(c) show droplet trajectories that are colored by particle velocity magnitude (m/s) at satellite droplet diameters of 18  $\mu$ m, 7  $\mu$ m and 3  $\mu$ m, respectively. Particle calculations are terminated at the carriage, the paper and other surfaces. The behavior of ink droplets becomes more complicated as ink droplets become smaller. Figure 6(d) shows droplet trajectories at a satellite droplet diameter of 5  $\mu$ m. We found



(a)



(b)

**Figure 8.** (a) Droplet trajectories for scans at 18 kHz. Droplet diameter is 5  $\mu$ m and initial velocity is  $-8$  m/s. Maximum flow velocity is 4.96 m/s. (b) Droplet trajectories for scans at 6 kHz. Droplet diameter is 5  $\mu$ m and initial velocity is  $-8$  m/s. Maximum flow velocity is 2.36 m/s.

that even small droplets could not circulate on the upstream side in a laminar flow. Numerical calculations also indicated that the upstream velocity component of droplets is necessary for mist to circulate on the upstream side.

We have extensively investigated mist circulation on the upstream side in a thermal ink jet printer using PIV (Particle Image Velocimetry). After we analyze these data, we will report further on this problem.

### Critical Diameter at Which Ink Droplets Dispersed

We generated 200 droplets and determined the critical diameter at which ink droplets dispersed. Figure 7 shows the critical diameter for droplet initial velocity. Large critical diameters are unstable for dispersed mist phenomenon. Figures 8(a) and 8(b) have droplet trajectories that are colored by particle velocity magnitude (m/s) for the scans at 18 kHz and 6 kHz for a diameter of 5  $\mu$ m. We set the initial y component velocity at  $-8$  m/s for both these cases. We found that the droplet velocity decreased abruptly for the scans at 6 kHz. We think that jetting frequency influenced misting in the following way. The air current generated by

**TABLE I. Ejection Conditions for Black Ink**

|                            | Main Droplet | Satellite 1 | Satellite 2 |
|----------------------------|--------------|-------------|-------------|
| Diameter ( $\mu\text{m}$ ) | 25.8         | 18          | 18          |
| Initial velocity (m/s)     | 12           | 10          | 8           |

**TABLE II. Thermal Ink Jet Operating Conditions For Analysis**

| Case   | Frequency | Carriage velocity | Main droplet flow rate (kg/s) | Satellite 1 flow rate (kg/s) | Satellite 2 flow rate (kg/s) |
|--------|-----------|-------------------|-------------------------------|------------------------------|------------------------------|
| Scan   | 18 kHz    | -0.57 m/s         | $1.428 \times 10^{-4}$        | $4.85 \times 10^{-5}$        | $4.85 \times 10^{-5}$        |
| Scan   | 9 kHz     | -0.57 m/s         | $7.14 \times 10^{-5}$         | $2.425 \times 10^{-5}$       | $2.425 \times 10^{-5}$       |
| Scan   | 6 kHz     | -0.57 m/s         | $4.76 \times 10^{-5}$         | $1.617 \times 10^{-5}$       | $1.617 \times 10^{-5}$       |
| Rescan | 18 kHz    | 0.57 m/s          | $1.428 \times 10^{-4}$        | $4.85 \times 10^{-5}$        | $4.85 \times 10^{-5}$        |
| Rescan | 9 kHz     | 0.57 m/s          | $7.14 \times 10^{-5}$         | $2.425 \times 10^{-5}$       | $2.425 \times 10^{-5}$       |
| Rescan | 6 kHz     | 0.57 m/s          | $4.76 \times 10^{-5}$         | $1.617 \times 10^{-5}$       | $1.617 \times 10^{-5}$       |

main drops tends to carry small misting droplets to the paper at higher frequencies. This is why misting is high at low frequencies. In a sense, the mist dispersal problem is physically the momentum transfer problem. The critical diameter becomes larger as the jetting frequency becomes lower. Thus, we find that large droplets are blown up at low frequencies. Spray flow is weak at low frequency, so relative velocity is large. Since there is considerable transfer of momentum from ink droplets to the flow field, it is easy for droplets with the same diameter to disperse. We can also comprehend that the drag force proportional to the relative velocity governs momentum transfer. In contrast, since the spray is strong at high frequency, the relative velocity is small. Therefore, it is not easy for the same droplet diameter to disperse at high frequency. The critical diameter is larger at low initial velocity. Increasing the initial velocity of droplets effectively solves the mist dispersal problem, because the critical diameters are small. Comparing the scans at 18 kHz with those at 6 kHz, we found that the small y component flow velocity facilitated the mist dispersal.

We adjusted the carriage velocity to -1.14 m/s for the scans at 18 kHz. We found that the relative velocity is small and the critical diameter tends to be large at a carriage velocity of -1.14 m/s, compared to the carriage velocity at -0.57 m/s.

## Summary

We investigated the mist dispersal phenomenon and discovered the following:

- Numerical calculations indicated vortices in the neighborhood of the nozzles. These calculations correlated well with the experimental results.
- Droplet motion depended on droplet diameter (Figs. 6(a) – 6(c)).
- A large vorticity region appeared on the upstream side despite carriage motion.
- At the same frequency, both the maximum velocity and maximum vorticity were large for the rescans.
- Mist could not circulate on the upstream side in a laminar flow. A physical mechanism is necessary for mist to circulate on the upstream side.
- Increasing the initial velocity of droplets effectively solves the mist dispersal problem, because the critical diameters are small.

**TABLE III. Maximum Values for Magnitudes of Velocity and Vorticity**

| Case          | Velocity (m/s) | Vorticity ( $\text{s}^{-1}$ ) |
|---------------|----------------|-------------------------------|
| Scan 18 kHz   | 4.96           | 17102                         |
| Scan 9 kHz    | 3.29           | 12374                         |
| Scan 6 kHz    | 2.36           | 10683                         |
| Rescan 18 kHz | 5.11           | 17413                         |
| Rescan 9 kHz  | 4.62           | 13233                         |
| Rescan 6 kHz  | 3.32           | 10856                         |

**TABLE IV. Average Velocity at Four Positions in Ink Tank**

| Position | Average velocity (m/s) |
|----------|------------------------|
| Black    | 0.685                  |
| Cyan     | 0.491                  |
| Magenta  | 0.483                  |
| Yellow   | 0.521                  |

- The drag force proportional to the relative velocity governs momentum transfer. Since the spray is weak at low frequency, the relative velocity is large. We found that the air current generated by main drops tends to carry small misting droplets to the paper at higher frequencies. This explains why misting is high at low frequencies.

Numerical calculations correlated well with the results obtained from mist dispersal experiments. Simply speaking, a steady flow field is generated through the interaction of ink droplets. Small satellite droplets have to be blown up by the flow field. We found that momentum exchange and the relative velocity of the flow field were significant factors in dispersing mist. To conclude, we found that the nonlinear coupling between the flow field and ink droplets defined the properties of the mist dispersal phenomenon.  $\triangle$

**Acknowledgment.** I am sincerely grateful to all my colleagues who helped me in one way or another to finish this work. Names that I need to mention include Dr. E. Mariano Freire, Mr. Les Dudek, Dr. Andrew Yeh, Mr. Masahiko Fujii, Mr. Tohru Mihara, Mr. Nobuyuki Hirooka and Mr. Kenji Ikeda. I am also indebted to Mr. Yutaka Miura of Fluent Asia Pacific Co., Ltd. and Dr. Mingkai Niu of Fluent Inc. for their technical explanations of FLUENT.

## References

1. B. L. Cooper, J. G. Patrick, D. R. Bloyer, L. G. Neubauer, and R. K. Beretta, US Patent 5,774,141 (1998).
2. A. Blumberg and R. Semiat, Velocity Measurements of Ink Drops Ejected from a Piezoelectric DOD Print Head-I. Technique Presentation, *J. Imaging Sci. Technol.* **46**, 171 (2002).
3. R. Semiat, Private Communication, 2002.
4. A. Asai, T. Hara and I. Endo, One-dimensional Model of Bubble Growth and Liquid Flow in Bubble Jet Printers, *Jpn. J. Appl. Phys.* **26**, 1794(1987).
5. F. J. Wang, P. Morehouse, J. F. Knapp, and G.A. Domoto, Hydrodynamics of Reverse Metering Flows, *J. Imaging Sci. Technol.* **42**, 562 (1998).
6. J. Q. Feng, A General Dynamic Analysis of Drop Ejection in Drop-on-Demand Ink Jet Devices, *J. Imaging Sci. Technol.* **46**, 398(2002).
7. M. H. Lean, Virtual Pixels Printed with Acoustic Mist Imaging, *J. Imaging Sci. Technol.* **46**, 216(2002).
8. E. M. Freire, Private Communication, 2002.
9. Fluent Inc., FLUENT 5 User's Guide Vol.3, 1998, Chap. 14.
10. M. Fujii, T. Hamazaki and K. Ikeda, New Thermal Ink Jet Printhead with Improved Energy Efficiency Using Silicon Reactive Ion Etching, *J. Imaging Sci. Technol.* **43**, 332(1998).